ARTICLE

A unified approach for determining the strength of Frc members subjected to torsion—Part I: Experimental investigation

Luca Facconi[1] 🟢 | Ali Amin[2] 🟢 | Fausto Minelli[1] 🟢 | Giovanni Plizzari[1] 🟢

[1]Department of Civil, Environmental, Architectural Engineering and Mathematics (DICATAM), University of Brescia, Brescia, Italy

[2]School of Civil Engineering, The University of Sydney, Sydney, Australia

Correspondence
Fausto Minelli, Department of Civil, Environmental, Architectural Engineering and Mathematics (DICATAM), University of Brescia, Brescia, Italy.
Email: fausto.minelli@unibs.it

Abstract

The strength and behavior of fiber reinforced concrete (FRC) members subjected to torsion has received little attention in the literature. The primary objective of including fibers in concrete is to bridge cracks once they form, and in doing so, provide some post-cracking resistance to the otherwise brittle concrete. This and the accompanying paper that follows present the results of a comprehensive experimental and analytical study aimed at describing the behavior and strength of FRC members subjected to torsion. In this paper, results are presented on large scale pure torsion tests which have been conducted on eighteen 2.7 m long by 0.3 m wide by 0.3 m high beams with varying transverse and longitudinal reinforcement ratios along with varying steel fiber types and dosages. The results of this study demonstrates that the addition of steel fibers significantly increases the stiffness, rigidity and the maximum resisting torque and maximum twist when compared to the same specimen without fibers. The addition of fibers substantially reduced crack widths and crack spacings induced by torsion. The complementary behavior of specimens containing fibers and stirrups is explored along with a critical discussion on members containing low amounts of conventional longitudinal and/or transverse reinforcement.

KEYWORDS

crack spacing, crack width, digital imagine correlation, experimental tests, fiber reinforced concrete, low reinforcement ratio, torsion, torsional rigidity

1 | INTRODUCTION

Torsion is a core stress resultant, and despite almost all concrete structures being subjected to torsion in some capacity, the design of reinforced concrete for torsion typically receives little attention. Some codes of practice[1] suggest that torsion can be dealt with at the ultimate

limit state by providing a minimum amount of reinforcement in the form of stirrups and longitudinal reinforcement bars to prevent excessive cracking. Although this method can lead to safe solutions, this prescriptive approach can lead to unnecessarily large amounts of costly, manually placed, transverse reinforcement within concrete structures.

It is well accepted that the use of randomly orientated and uniformly distributed steel fibers within concrete significantly improves the post-cracking behavior of concrete.[2–5] Several experimental and analytical campaigns over the last few decades have clearly demonstrated the effectiveness of fibers in resisting shear[6–10] and flexure[11–17] in large scale structural elements. Recent studies have also demonstrated that the inclusion of fibers can also significantly improve the serviceability behavior of concrete structures.[18–23] However, despite the well-known beneficial properties of steel fiber reinforced concrete (SFRC) in academia, its adoption in practice has typically been taken up in non-load bearing elements for the control of cracking or where the placement of reinforcement is problematic. Codes of practice such as[24–28] indeed contain detailed and accepted methods which are capable in predicting the strength of SFRC elements subjected to shear and flexure. However, despite the wider community appreciating that the presence of fibers increases the capacity of reinforced concrete in resisting torsion, as experimentally demonstrated by several research programs,[29–35] design guidelines are unavailable to the practicing engineer.

To that end, this and the accompanying paper[36] present the results of a comprehensive experimental and analytical study aimed at describing the behavior and strength of SFRC members subjected to torsion. This paper specifically describes and reports on an experimental study where eighteen large-scale fiber reinforced concrete beams were tested in pure torsion. The specimens within the test series had varying transverse and longitudinal reinforcement ratios along with varying steel fiber types and dosages. The tests were complemented with a full suite of material characterization tests to fully quantify the post cracking behavior of the FRC. The results presented in this paper provide experimental background to inform the theoretical models developed in the accompanying paper.[36]

2 | EXPERIMENTAL PROGRAM

2.1 | Specimen properties

A total of eighteen SFRC beams were cast and tested in pure torsion. Details of each specimen are provided in

TABLE 1 Main properties of beam specimens

Test series	Specimen	Material ID	$\varnothing_l$ (mm)	ρ_l (%)	Stirrups $\varnothing_{st}/s_{st}$ (mm/mm)	ρ_{st} (%)	Fiber content (kg/m³)	ρ_f (%)
1	TB1-PC-L18	PC1	18	1.13	—	—	—	—
1	TB2-PC-L18-ST6/110	PC1	18	1.13	6/110	0.17	—	—
1	TB3-G25-L18	FRCG25	18	1.13	—	—	25	0.32
1	TB4-G25-L18	FRCG25	18	1.13	—	—	25	0.32
1	TB5-G50-L18	FRCG50	18	1.13	—	—	50	0.63
1	TB6-G50-L18	FRCG50	18	1.13	—	—	50	0.63
2	TB7-D25-L18	FRCD25	18	1.13	—	—	25	0.32
2	TB8-D25-L18	FRCD25	18	1.13	—	—	25	0.32
2	TB9-D50-L18	FRCD50	18	1.13	—	—	50	0.63
2	TB10-D50-L18	FRCD50	18	1.13	—	—	50	0.63
2	TB11-D50-L18-ST6/150	FRCD50	18	1.13	6/150	0.13	50	0.63
2	TB12-D50-L18-ST6/150	FRCD50	18	1.13	6/150	0.13	50	0.63
2	TB13-PC-L18-ST6/150	PC2	18	1.13	6/150	0.13	—	—
2	TB14-PC-L18-ST6/150	PC2	18	1.13	6/150	0.13	—	—
2	TB15-D50-L18-ST6/200	FRCD50	18	1.13	6/200	0.09	50	0.63
2	TB16-D50-L18-ST6/200	FRCD50	18	1.13	6/200	0.09	50	0.63
2	TB17-D50-L8	FRCD50	8	0.22	—	—	50	0.63
2	TB18-D50-L8	FRCD50	8	0.22	—	—	50	0.63

Note: The test series 1 refers to specimens tested in a previous study[35] while Test series 2 concerns to the beams tested in the present study.
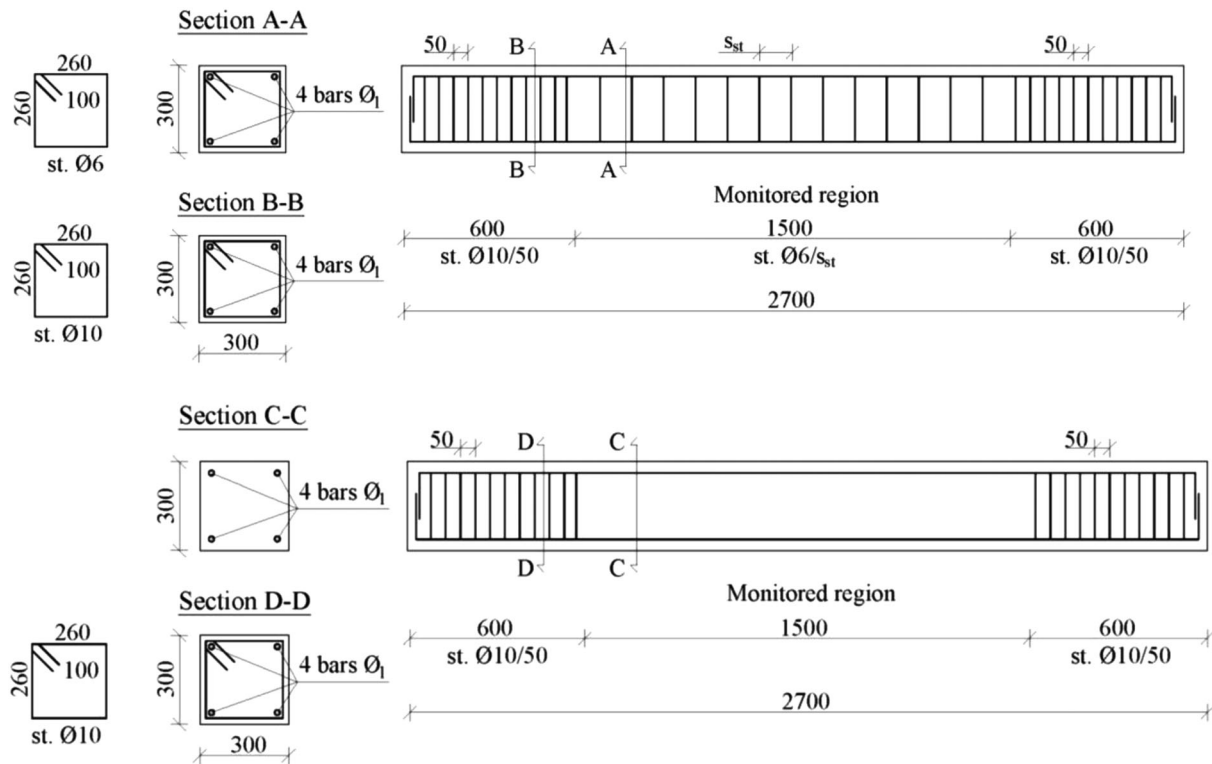
FIGURE 1 Schematic of the specimens (dimensions in mm)

Table 1 and Figure 1. The specimens were cast over two series. The first series of specimens (Series 1) were tested in a previous study.[35] The results of specimens constituting Series 1 are reported here for comparison purposes. Both Series 1 and Series 2 consisted of specimens having the same geometry, but varied steel fiber dosages and conventional reinforcement (transverse and longitudinal) ratios. The specimens are designated using the four/five index notation: *TBW-X-Y-Z*, where "*TB*" refers to "Torsion Beam," "*W*" is the specimen number (which ranges from 1–18), "*X*" refers to either "PC" for plain concrete or "G#/D#" (where G/D refers to the fiber type [details provided in Table 2] and # is the fiber dosage in kg/m^3), "*Y*" is "L" followed by either 8 or 18 which refers to the diameter of the longitudinal reinforcement ($\varnothing_l$), and "*Z*" is included in the index if the specimen contains stirrups. If the specimen contains stirrups, then the numbers succeeding the term "ST" are the diameter and the spacing of the 2-legged stirrups. For example, specimen TB12-D50-L18-ST6/150 represents Torsion Beam 12, containing 50 kg/m^3 of fiber type D, 18 mm diameter longitudinal reinforcement, and 6 mm 2-legged stirrups spaced 150 mm c/c contained within the monitored region of the beam.

Also contained in Table 1 are the longitudinal ($\rho_l = A_{sl}/A_c$) and the transverse ($\rho_{st} = A_{st}/[b \times s_{st}]$) reinforcement ratios as well as the volumetric dosage of fibers (ρ_f).

We note that ρ_l is calculated as the ratio of the total cross-sectional area of the longitudinal rebars (A_s) to the gross cross-sectional area ($A_c = b$ (base) $\times h$ (height) $= 300 \times 300 = 9 \cdot 10^4$ mm^2) of the beams while s_{st} is as the average spacing between the stirrups located in the monitoring region (Figure 1).

One of the key aspects considered in this study is the behavior of lightly conventionally reinforced (transverse and longitudinal) FRC members subjected to torsion. Aside of specimen TB1, all other specimens contained varying amounts of reinforcement in the form of fibers and/or stirrups. Specimens TB2, TB13 and TB14 were composed of plain concrete and were reinforced with transverse reinforcement ratios and spacings very close to the minimum values recommended by Eurocode 2[37] (i.e., $\rho_{st,min} = 0.1\%$ and $s_{st,min} = 150$ mm). It is worth noting that, except for specimens TB1 and TB2, two specimens for each beam typology were tested in order to mitigate measurement uncertainties.

2.2 | Material properties

Two different concrete mix designs were used to cast the beams tested in this study. Details of the concrete composition are presented in Table 2 where Test Series 1 corresponds to beams TB1-TB6 and Test Series 2 corresponds

TABLE 2 Concrete composition and properties of steel fibers

Test series	1	2
Material	PC1, FRCG25, FRCG50	PC2, FRCD25, FRCD50
Cement type	CEM I 42.5R	CEM II 32.5R
Cement content (kg/m^3)	380	420
Fine aggregate 0–4 mm (kg/m^3)	1082	1000
Coarse aggregate 4–20 mm (kg/m^3) (kg/m^3)	742	815
Water-cement ratio	0.5	0.42
Super plasticizer (l/m^3)	0.37 (PC1) 0.74 (FRCG25) 1.85 (FRCG50)	0.86
Fiber ID	G	D
Fiber shape	Hooked-end	Hooked-end
Material	High carbon, cold drawn steel	High carbon, cold drawn steel
Tensile strength (MPa)	>2200	>2300
Length l (mm)	30	60
Diameter Ø (mm)	0.35	0.9
Aspect ratio l/Ø	86	65
Fiber view		

to beams TB7-TB18. Concrete rheology's for each test series were based on each having the same maximum aggregate size (and type) and on slightly different cement contents. The dosage of each component of the concrete was selected to obtain a target characteristic cylindrical compressive strength (f_{ck}) of 35 MPa for each test series.

For Test Series 1, the SFRC beams were manufactured over three separate pours. The first pour comprised of beams TB1 and TB2; the second pour comprised of beams TB3 and TB4; and the third pour comprised of beams TB5 and TB6. Specific details can be found in Reference 35.

For Test Series 2, the SFRC beams were manufactured in a single pour. TB13 and TB14 were cast first. The calculated weight of the steel fibers required to increase the fiber dosage to 25 kg/m^3 was added, on-site, and mixed thoroughly in the concrete agitator for 5 min. Specimens TB7 and TB8 were then cast along with the material companion samples (i.e., cubes, prisms, and round panels). Next, the calculated weight of the steel fibers required to increase the fiber dosage to 50 kg/m^3 was added to the agitator and mixed thoroughly again for 5 minutes. All remaining specimens were then cast. The properties of the hooked-end steel fibers added to the different batches are reported in Table 2.

Following casting, the large-scale beams were kept in their timber molds for at least 7 days. The specimens were moist cured in this period and were covered with a polyethylene sheet in order to minimize water evaporation. At the end of this first curing phase, the beams were stripped from their molds and then left on the laboratory floor under ambient temperatures (approximately 20°C) until time of testing.

The companion material specimens (i.e., cubes, prisms and round panels) were all demolded after 24 h of moist curing. They were then all placed in a controlled climate chamber at a constant temperature and relative humidity of 20 C and at 90%, respectively.

Table 3 summarizes the mean mechanical properties and the corresponding coefficient of variations (values in round brackets) obtained from the characterization tests performed on the concrete mixes. The number of specimens tested for each test is also provided in Table 3. The uniaxial cubic compression tests were performed on 150 mm cubes after at least 28 days of curing. These tests provided the mean cube strength, $f_{cm,cube}$. The corresponding cylinder compressive strength is taken as $f_{cm} = 0.83 \cdot f_{cm,cube}$, which in turn provided the mean uniaxial tensile strength ($f_{ctm} = 0.3 f_{cm}^{2/3}$). The mean secant elastic modulus ($E_{cm} = 22 \cdot [f_{cm}/10]^{0.3}$) was calculated according to Eurocode 2.[37]

The post cracking behavior of the concrete was assessed by testing $150 \times 150 \times 500$ mm^3 notched prisms under 3-point bending (3PBTs). These prisms were tested

TABLE 3 Concrete properties

Test series	1	1	1	2	2	2
Material ID	PC1	FRCG25	FRCG50	PC2	FRCD25	FRCD50
Specific gravity (kg/m^3)	2425	2480	2440	2412	2451	2443
Fiber content (kg/m^3)	0	25	50	0	25	50
Fiber volume fraction (ρ_f) (%)	0	0.32	0.63	0	0.32	0.63
Uniaxial compression test on cubes (compressive strength)						
# of cubes	12	12	12	8	7	8
$f_{cm,cube}$ (MPa)	43.5 (7.1%)	52.6 (6.1%)	52.3 (7.9%)	49.5 (6.2%)	51.6 (3.7%)	51.3 (4.3%)
f_{cm} (MPa)	36.1	43.6	43.4	41.1	42.8	42.6
f_{ck} (MPa)	31.0	38.4	36.7	36.0	39.7	39.4
f_{ctm} (MPa)[a]	3.0	3.4	3.3	3.3	3.5	3.5
E_{cm} (GPa)[a]	32.3	34.2	34.2	33.6	34.0	34.0
Three point bending test (3PBT)						
# of prisms	6	12	6	4	6	7
f_L (MPa)	4.4 (9.6%)	5.0 (12.4%)	6.0 (9.1%)	4.1 (11.5%)	4.29 (7.8%)	4.7 (8.6%)
f_{R1} (MPa)	—	4.1 (22.6%)	7.2 (16%)	—	3.4 (41%)	6.0 (30.8%)
f_{R2} (MPa)	—	4.5 (24.1%)	7.2 (9.4%)	—	5.2 (44.3%)	7.8 (15.8%)
f_{R3} (MPa)	—	4.2 (23.5%)	6.6 (9.5%)	—	5.03 (36.3%)	6.7 (14.7%)
f_{R4} (MPa)	—	3.8 (22.7%)	5.7 (10%)	—	4.8 (28.4%)	6.1 (12.6%)
FRC class[b]	—	2c	5c	—	1e	2.5e

Coefficient of variation reported in round brackets (CV%).

[a]Calculated according to Eurocode 2.

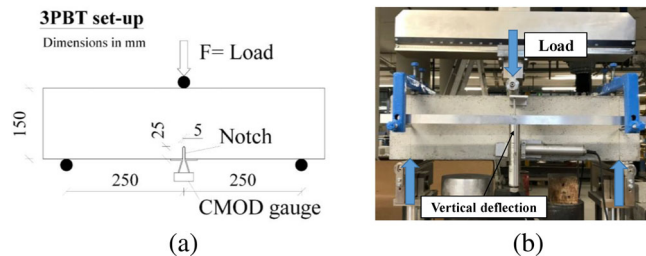[b]FRC classification according to *fib* Model Code 2010[1].

FIGURE 2 Three-point bending test set-up according EN 14651[38]: (a) schematic; (b) view of a FRCG25 notched beam under testing

according to EN 14651[38] (see Figure 2). Based on the tensile stress-*CMOD* (Crack Mouth Opening Displacement) curves resulting from the 3PBTs (see Figure 3), the mean residual strengths required by the *fib* Model Code 2010 (MC2010)[1] were defined. These include the limit of proportionality f_L (i.e., the greatest flexural tensile strength attained for *CMOD* ranging from 0 to 0.05 mm) and the residual strengths f_{R1} (*CMOD* = 0.5 mm), f_{R2} (*CMOD* = 1.5 mm), f_{R3} (*CMOD* = 2.5 mm), and f_{R4} (*CMOD* = 3.5 mm). As also required by the MC2010, the characteristic values of the residual strengths were used to determine the FRC class for each FRC mix (see Table 3).

Figure 3 reports the flexural stress—*CMOD* results exhibited by the notched beams for each of the two test series. Contained within each figure are the individual results of each prism tested along with the mean curves which were obtained by averaging all the curves corresponding to the same SFRC typology. For specimens within Test Series 1, the residual strengths of the concrete made with 50 kg/m^3 of "G" fibers (i.e., FRCG50) were about 50–75% greater than those of the concrete containing 25 kg/m^3 of "G" fibers (FRCG25) (see Table 3). A slightly higher scatter in results was observed for the prisms tested in Test Series 2, in which the residual strengths of FRCD50 were approximately 27–76% greater than FRCD25. By comparing the average curves of Test Series 1 (Figure 3a) with those of Test Series 2 (Figure 3b), the structural performance of the two types of fibers adopted can be highlighted. Regarding the materials containing 25 kg/m^3 of fibers, fiber type "D" provided FRCD25 with residual strengths f_{R2}, f_{R3} and f_{R4} that were 14–26% greater than those attained by concrete FRCG25 containing fiber type "G." On the contrary, the residual strength f_{R1} of FRCD25 was about 20% lower than that of FRCG25. When comparing the SFRC reinforced with 50 kg/m^3 of fibers, it appears that fiber
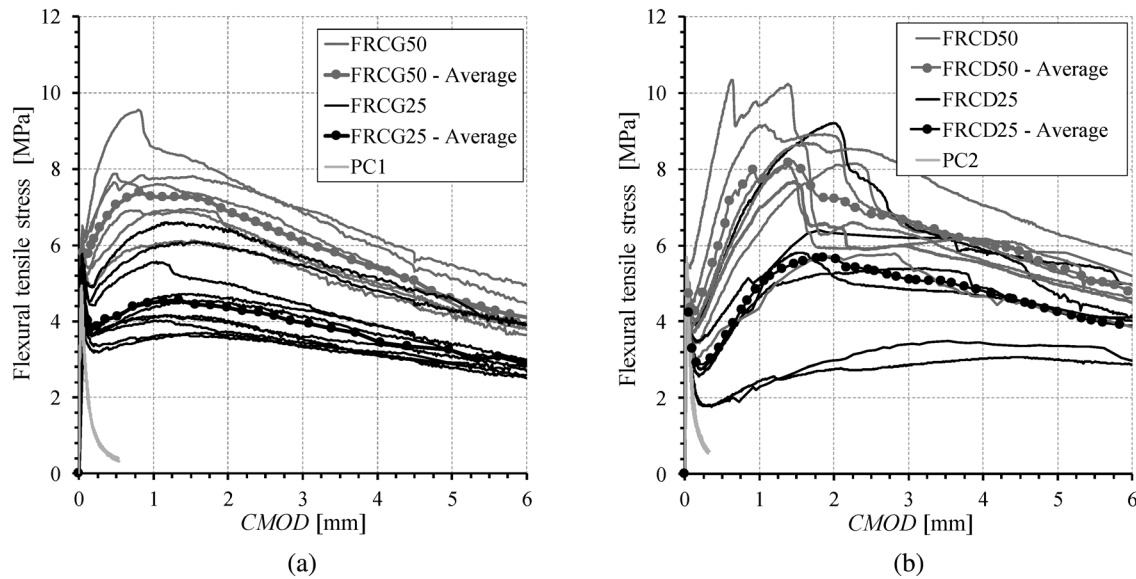
FIGURE 3 Flexural tensile stress-CMOD curves from three point bending tests according EN 14651[38]: test series 1 (a) and 2 (b)

type "G" provided FRCG50 with a 20% greater residual strength, as defined by f_{R1}, than that exhibited by FRCD50. For *CMOD* values higher than 0.5 mm, the strength of FRCD50 was generally no more than 8% greater than that of FRCG50. As expected, the shorter length of fiber type "G" (length = 30 mm) when compared to fiber type "D" (length = 60 mm) resulted in a higher residual tensile strength right after the onset of crack formation (i.e., when the *CMOD* was less than 1.5 mm). This consideration explains the higher values of f_{R1} attained by both FRCG25 and FRCG50 relative to FRCD25 and FRCD50.

It is worth noting that the material characterization beams composed of FRCD25 were affected by a scatter of results approximately twice as much as the FRCD50 specimens. Following testing of all 3PBTs, the number of fibers crossing the cracked plane were counted. The high scatter of the data was probably due to the non-uniform distribution of fibers within 3 of the 6 FRCD25 beams.

Table 4 summarizes the main mechanical properties of the deformed (longitudinal and transverse) reinforcement used to reinforce the large-scale torsion beams. In more detail, Table 4 reports the nominal diameter of conventional reinforcement ($Ø_l$), the mean yield strength (f_y), the maximum tensile strength (f_{su}), and the corresponding strain at ultimate strength (ε_{su}). These parameters were obtained by performing uniaxial tension tests on reinforcement samples in accordance with ISO 15630-1.[39]

2.3 | Test set-up and instrumentation

The large-scale torsion tests were loaded using the test rig schematically illustrated in Figure 4a. The rig was used in a recent study and its specific details can be found in Reference 35. In short, each test specimen was laid on two steel rollers placed approximately 2460 mm apart.
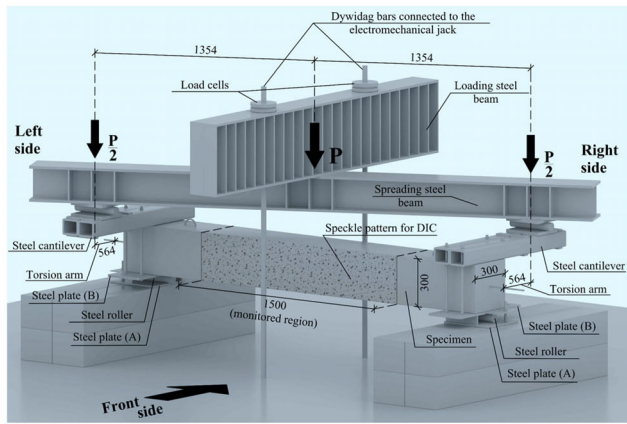
TABLE 4 Properties of steel deformed rebars

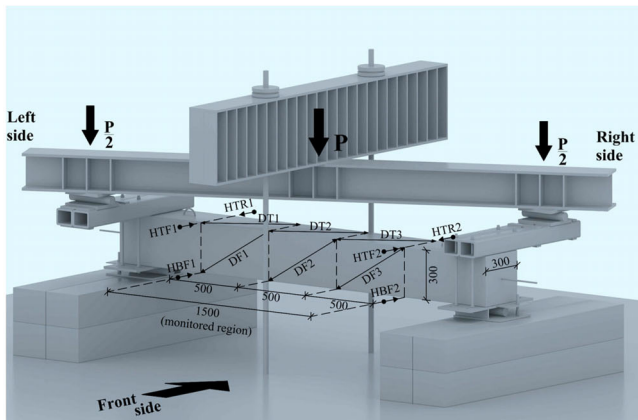| Test series	Reinforcing bar type	# of rebar samples	Diameter ($Ø_l$) (mm)	f_y (MPa)	f_{su} (MPa)	ε_{su} (%)
1	Ø6[a]	4	6	485 (1.9%)	597 (0.42%)	15.6 (14%)
2	Ø6[b]	6	6	549 (6.8%)	609 (2.1%)	2.3 (15.1%)
2	Ø8[a]	3	8	567 (1.1%)	660 (1.1%)	10.5 (9.1%)
1	Ø10[a]	4	10	524 (2.1%)	660 (1.5%)	12.6 (10%)
2	Ø10[a]	3	10	552 (1.3%)	670 (0.9%)	9.6 (6.3%)
1	Ø18[a]	4	18	516 (2.0%)	659 (2.7%)	17.7 (11%)
2	Ø18[a]	3	18	507 (0.1%)	612 (0.4%)	9.3 (4.1%)

Coefficient of variation reported in round brackets (CV%).
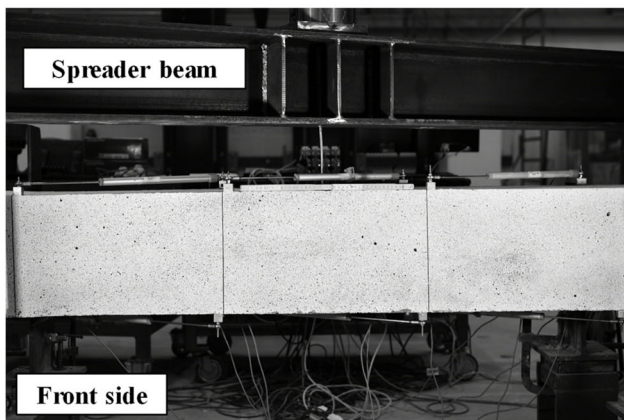
[a]Hot rolled deformed rebars.

[b]Deformed rebars obtained from hot-rolled and cold-drawn steel coils.

bolts. The beam-to-plate (B) and the beam-to-cantilever interfaces were both filled with a thin layer of high strength, low shrinkage mortar to prevent either contact problems or relative movement between the cantilevered arms and the specimen. A spreader beam was used to apply the loads ($P/2$) to each of the steel cantilevers which generated the two equal counteracting torques (T). The total load (P) was monitored using two load cells connected to the loading beam. A 1000 kN capacity electromechanical thrust jack was used apply the total load.

The applied load was increased monotonically at a constant speed such that the unit angle of twist of the specimen increased at a rate equal to approximately 0.01 rad/(m·s). To measure the rotation at the ends of the monitored region, horizontal potentiometers were positioned on the front left side (i.e., HTF1, HBF1), on the front right side (i.e., HTF2, HBF2), on the back left side (i.e., HTB1, HBB1) and on the back right side (i.e., HTB2, HBB2) of the specimen (refer to Figure 4a). A total of 3 linear diagonal potentiometers (e.g., see the instruments named as DF and DT in Figure 4a) were installed on each side of the beam to detect the progressive formation of cracks.

In order to get an accurate assessment of the crack development, including the precise measurement of the width and inclination along entire cracks during the test, a 2D Digital Image Correlation (DIC) technique[40] was used to monitor the front side of some of the specimens (i.e., TB8, TB10, TB12, TB14, TB16, TB18). We note that the potentiometers were not installed on the front side of the beam when the DIC system was used. The specimens monitored with the DIC system were prepared by first applying a thin layer of white paint to the surface of the specimen. This base layer was then sprayed with black paint to generate a stochastic speckle pattern on its surface (see Figure 4b). The density of the pattern was adapted to the size of the beam. To record HD digital images, a 46 Megapixel Nikon high-resolution camera was mounted on a tripod with its axis perpendicular to the beam side. The system captured photos every 5 s. Finally, the commercial software Optecal® (www.optecal.com) was used to analyze the photos taken during the test. The strains and displacements of the investigated side of the beam were determined in 2D space. On the contrary, the actual deformations resulting from the applied torsion involve movement in three dimensions. Despite this, the authors believe that the DIC 2D measurements can be considered reliable, provided that the angle of twist of the specimen is not too large. The latter condition usually occurs in the pre-peak stage of the global torsional response.

FIGURE 4 (a) Schematic of the loading configuration and (b) of the instrumentation set-up. (c) View of the speckle pattern adopted to monitor the crack formation using DIC on some of the tested beams. (Dimensions in mm)

Each roller allowed the beam to freely rotate about its longitudinal axis, without preventing extension or contraction due to the applied torsion. A couple of steel cantilevers were positioned on each side of the specimen. These steel members were secured to the bottom steel plates (B) using four high-strength steel
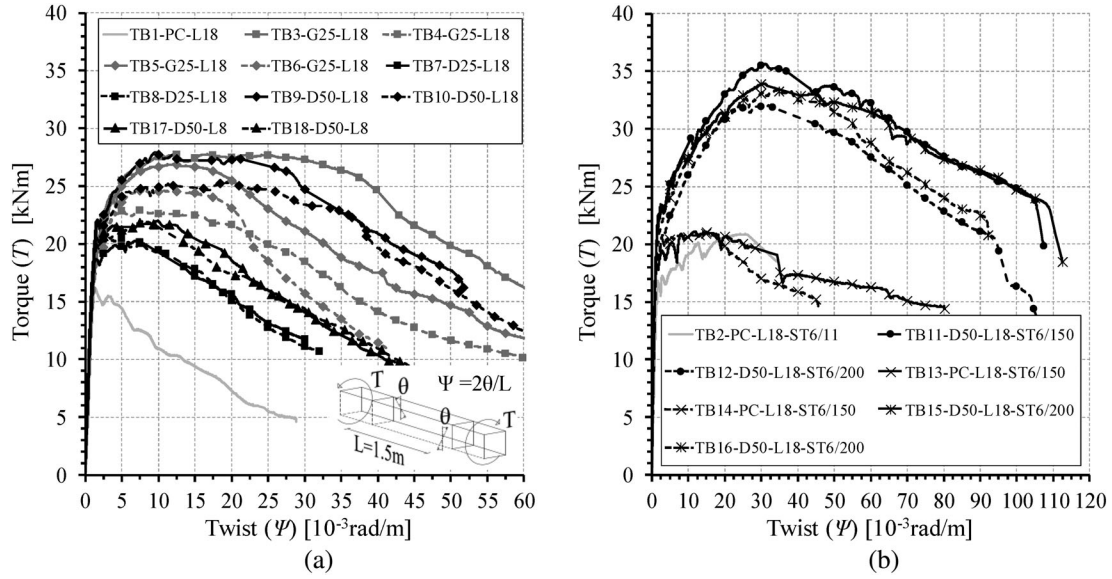
FIGURE 5 Torque vs. twist response: (a) beams without stirrups; (b) beams with stirrups

3 | TEST RESULTS AND DISCUSSION

3.1 | Torque—twist response

Figure 5 presents the torque (T) vs. twist (Ψ) responses for each of the tested beams. For the sake of convenience, the gray curves refer to the specimen of the Test Series 1 whereas the black curves correspond to the beams tested as part of Test Series 2. All specimens exhibited a similar linear response from initial loading to the formation of the very first cracks. The initial torsional rigidity ($K_{el,exp}$) as well as the torque (T_{cr}) and the corresponding twist (Ψ_{cr}) at first cracking for each specimen are summarized in Table 5. We note that $K_{el,exp}$ is defined as the slope of the T–Ψ response between initial loading and first cracking.

With the exception of the concrete used to manufacture specimens TB1 and TB2 (i.e. concrete mix PC1), the mean elastic modulus (E_{cm}) of the materials used in the present research was approximately equal to 34 GPa (see Table 3). According to the de Saint-Venant's (DSV) theory, the expected elastic torsional rigidity (K_{DSV}) is equal to:

$$K_{DSV} = G_{cm} \cdot J_t = 16,130 \text{ kNm}^2/\text{rad} \quad (1)$$

where $G_{cm} = E_{cm}/[2(1 + \nu)] = 14.2$ GPa is the shear modulus of concrete; $\nu = 0.2$ is the Poisson's ratio of the concrete; $J_t = bh^3/[3 + 4.1(h/b)^{3/2}] = 1.141 \ 10^9 \text{ mm}^4$ is the polar moment of inertia of the cross section; and $b = h = 300$ mm are the width and the depth of the cross section, respectively. This rigidity is about 11% lower than

the mean value of initial elastic rigidity (i.e., $K_{el,exp,mean} = 18,155 \text{ kNm}^2/\text{rad}$ [CV = 12%]) exhibited by the 16 specimens not manufactured with PC1. The latter had an elastic modulus of $E_{cm} = 32.3$ GPa, which corresponds to a shear modulus of $G_{cm} = 13.5$ GPa. By Equation 1, $K_{DSV} = 15,330 \text{ kNm}^2/\text{rad}$ for specimens TB1 and TB2. This is very close to the mean rigidity (i.e., $15,650 \text{ kNm}^2/\text{rad}$ [CV = 2%]) observed in the experimental tests.

The experimental values of T_{cr} (Table 5) appear very consistent and are characterized by a limited scatter. In fact, by averaging the values of T_{cr} reported in Table 5, a mean cracking torque of 13.1 kNm is obtained, with a CV of 8.4%. We note that the addition of fibers does not significantly affect the torque at first cracking (since fibers are activated after cracking of the concrete matrix). Based on the mean tensile strength of concrete (f_{ctm}—see Table 3), the DSV theory provides the following relationship to estimate the torque at first cracking for the specimens:

$$\begin{aligned} T_{cr,DSV} &= f_{ctm} \cdot \frac{b \cdot h^2}{3 + 1.8h/b} \\ &= (\text{min}) \ 16.9 \\ &\div (\text{max}) \ 19.7 \text{ kNm} \ (\text{Mean} = 18.8 \text{ kNm}) \end{aligned} \quad (2)$$

where the minimum and maximum values of the torque reported in Equation (2) correspond to the lowest (3.0 MPa) and the highest (3.5 MPa) obtained value of f_{ctm}, respectively. The mean cracking torque (18.3 kNm) resulting from the DSV theory is about 40% greater than that (13.1 kNm) observed from testing.

The occurrence of the first diagonal crack on one face of the beam did not significantly affect the initial stiffness

TABLE 5 Summary of main experimental results

Specimen	$K_{el,exp}$ $\left(\frac{kNm^2}{rad}\right)$	T_{cr} (kNm)	Ψ_{cr} $\left(\frac{10^{-3} rad}{m}\right)$	T'_{cr} (kNm)	Ψ'_{cr} $\left(\frac{10^{-3} rad}{m}\right)$	T_p (kNm)	Ψ_p $\left(\frac{10^{-3} rad}{m}\right)$	$\Psi_{0.8}$ $\left(\frac{10^{-3} rad}{m}\right)$
TB1-PC-L18	15,900	12.40	0.78	16.18	1.30	16.18	1.30	6.25
TB2-PC-L18-ST6/110	15,400	13.08	1.06	16.67	1.81	20.84	24.35	34.1[a]
TB3-G25-L18	16,700	13.40	0.88	20.55	1.92	27.32	12.38	44.6
TB4-G25-L18	17,100	12.00	0.80	20.25	1.97	22.94	7.52	30.0
TB5-G50-L18	19,630	13.89	0.79	20.76	1.65	26.94	12.00	29.3
TB6-G50-L18	12,850	13.74	1.17	18.97	1.48	24.63	10.52	23.2
TB7-D25-L18	17,647	11.92	0.68	18.68	1.44	20.27	6.70	17.9
TB8-D25-L18	17,575	15.96	0.98	20.03	1.48	20.8	3.15	17.3
TB9-D50-L18	20,545	13.23	0.61	22.10	1.68	27.9	9.43	36.6
TB10-D50-L18	18,426	12.9	0.75	19.92	1.60	25.3	19.50	39.1
TB11-D50-L18-ST6/150	21,480	13.2	0.65	22.47	1.89	35.6	31.24	75.8
TB12-D50-L18-ST6/150	16,930	13.5	0.81	19.38	1.83	32.0	30.90	68.8
TB13-PC-L18-ST6/150	19,580	11.6	0.6	18.28	1.23	21.11	11.70	47.3
TB14-PC-L18-ST6/150	17,215	11.0	0.64	19.30	1.48	21.07	15.16	31.1
TB15-D50-L18-ST6/200	19,740	13.5	0.7	21.00	1.53	33.86	31.17	82.9
TB16-D50-L18-ST6/200	16,360	13.6	0.84	20.07	1.68	33.36	37.50	67.8
TB17-D50-L8	19,840	12.4	0.64	21.88	1.56	21.95	10.00	21.8
TB18-D50-L8	18,860	13.7	0.74	20.60	1.46	22.00	8.07	19.05

[a]Minimum post-peak torque ($0.89 \cdot T_p$) and corresponding twist of the specimen TB2-PC-L18-ST6/110.

of the specimen. On the contrary, once the first crack extended over to the adjacent sides of the specimen, and in doing so forming a continuum spiral, a reduction of the torsional stiffness appeared on the torque-twist response with a knee located at the end of the elastic branch of the curve. The torque and the twist corresponding to this change of stiffness are here named as T'_{cr} and Ψ'_{cr}, respectively (see Table 5). Except for the reference specimen (TB1), which exhibited a softening response after first cracking, all other specimens tended to increase in capacity after the attainment of T'_{cr}. The peak torque (T_p) and corresponding twist (Ψ_p) attained by each of the specimens are provided in Table 5. Figure 6a,b are provided to allow one to appreciate the increment of resisting torque in terms of the ratio T_p/T'_{cr} and the increment of the twist capacity with respect to the ratio $\Psi_{0.8}/\Psi'_{cr}$, where $\Psi_{0.8}$ is the twist recorded after the peak at $T = 0.80\ T_p$.

3.1.1 | Specimens without stirrups

The specimens without stirrups were provided with a relatively large amount of longitudinal reinforcement ($\rho_l = 1.13\%$) in order to better highlight the combined effect of

the fibers and stirrups. These specimens recorded torque increments ranging from a minimum of 1.04 to a maximum of 1.33 (refer to Figure 6a). Among the others, the specimens containing 50 kg/m³ of fibers recorded very similar increments of capacity, as defined above, that varied from 1.26 to 1.29 for specimens TB9 and TB6, respectively. For specimens reinforced with 25 kg/m³ of fibers, the increment of the resisting torque ranged from 1.04 (TB8) to 1.13 (TB4). Interestingly, specimen TB3 (with 25 kg/m³ of fibers "Type G") exhibited an unexpected over-strength when compared to the other specimens containing the same quantity of fibers. As will be described in Section 3.3, the relatively large amount of dispersed cracking surrounding the ultimate failure crack can partly explain the relatively superior performance of specimen TB3.

Regarding specimens TB17 and TB18, the very low amount of longitudinal reinforcement was expected to significantly increase the strain in the rebars, possibly close to yielding. As shown in Figure 6a, the high stress level developed in the longitudinal reinforcement led to a reduction in the increment of resistance presented by specimens TB17 and TB18. These were 21% and 16% lower than that achieved by the two specimens containing the same type and amount of fibers but with a larger longitudinal reinforcement ratio (i.e., specimens TB9 and TB10).
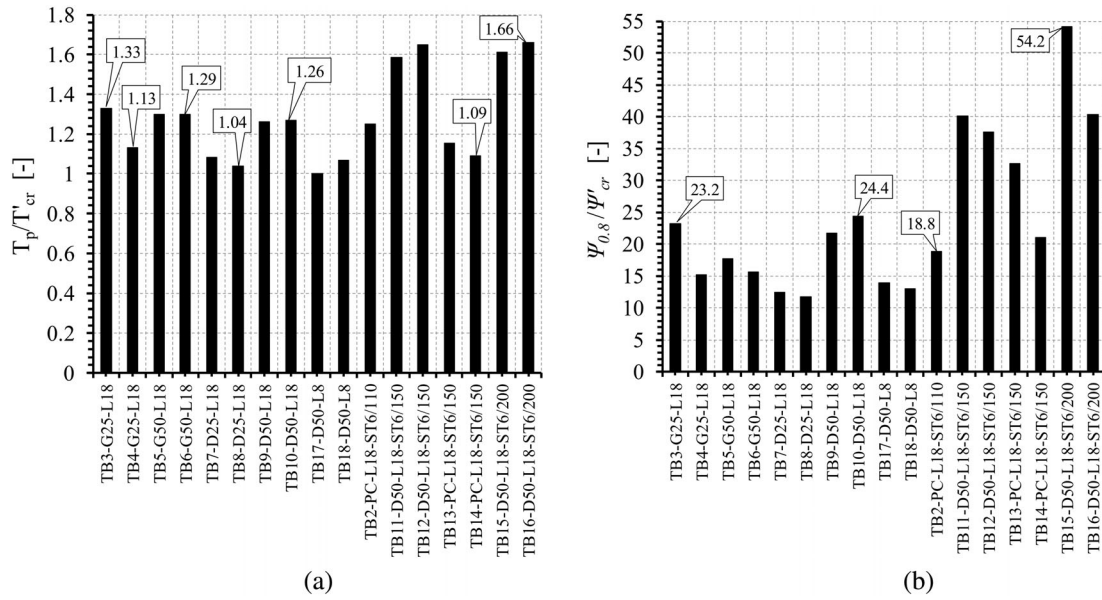
FIGURE 6 (a) Torque increment (T_p/T'_{cr}) after cracking. (b) Increment of the twist capacity ($\Psi_{0.8}/\Psi'_{cr}$) after cracking
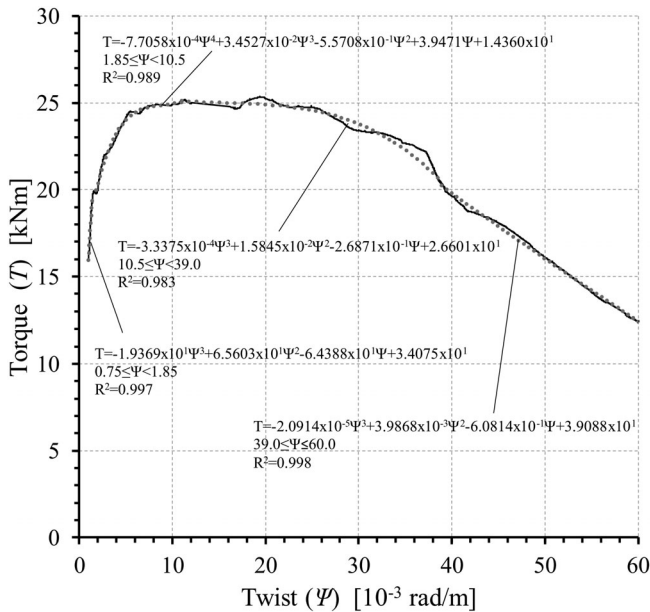

FIGURE 7 Polynomial interpolation of the torque vs. twist response of TB10-D50-L18

After crack localization, the global response (refer to Figure 5a) of the specimens typically presented a horizontal plateau followed by a descending branch. Referring to Figure 7b, it appears that all specimens had a ductile response as the twist increment varied from a minimum of 11.7, exhibited by specimen TB8, to a maximum of 23.2 attained by specimen TB3. In spite of the reduced longitudinal reinforcement ratio, the specimens TB17 and TB18 displayed significant ductility.

3.1.2 | Specimens with stirrups

Consistent with observations reported in the literature,[33,34] the combination of fibers and stirrups led to a significant improvement in the behavior of specimens subjected to torsion. This resulted in an increase in the torque resisted by the members along with the twist capacity of the specimens, relative to the reference samples not containing fibers (see Figure 5b). After cracking, the addition of fibers considerably mitigated the loss of torsional resistance that affected the response of the specimens manufactured without fibers and containing stirrups (i.e., TB2, TB13, TB14). Assuming yielding of the transverse reinforcement, by the space truss model, the latter reached a capacity more than 40% higher than that predicted by Collins and Mitchell's model[41]:

$$T_{st,CM} = 2A_o \cdot \frac{A_{sv} \cdot f_{sy,v}}{s_{st}} \cdot \cotan\theta_v$$
$$= \begin{cases} 14.3 \, \text{kNm} & (\text{beam TB2}) \\ 11.9 \, \text{kNm} & (\text{beams TB13 TB14}) \end{cases} \quad (3)$$

where $A_o = (b - t_c) \cdot (h - t_c) = 59{,}414 \, \text{mm}^2$ is the area enclosed by the centerline of the equivalent tube; $t_c = 0.75 A_c/p_c = 56.3 \, \text{mm}$ is the thickness of the equivalent tube; $A_{sv} = 28.3 \, \text{mm}^2$ is the cross sectional area of a single leg of the stirrups used in the tests; $f_{sy,v}$ is the yield strength of stirrups (see Table 4); s_{st} is the spacing of the transverse reinforcing (see Table 1); θ_v is the mean angle of inclination of cracks which is assumed equal to 45°. The underestimation of resistance when employing Equation (3) may be related to different phenomena not
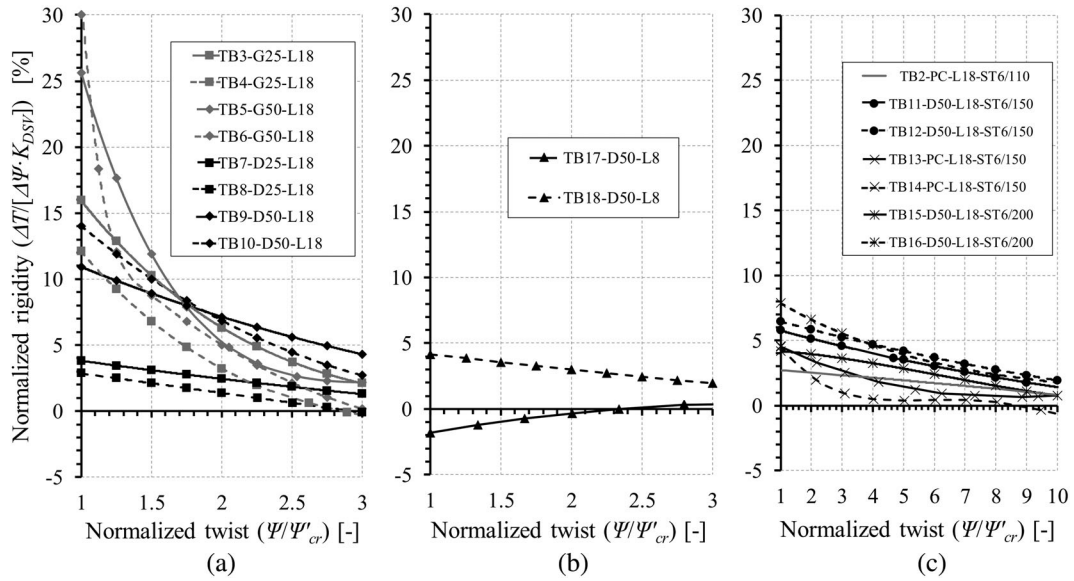
FIGURE 8 Normalized torsional rigidity vs. normalized twist: (a) specimens without stirrups; (b) specimens with low longitudinal reinforcement ratios; (c) specimens with stirrups

considered by the model, e.g. the aggregate interlock mechanism as well as the tensile rupture of the stirrups that governed the ultimate behavior of the test beams. One should also consider that the value of t_c significantly affects the calculated torque. Regarding this factor, the Eurocode 2 suggests a tube thickness (i.e., $t_c = A_c/p_c$) 33% greater than that adopted herein.

The effect of fibers on the strength of the beams with stirrups is well highlighted in Figure 5b. The increment of strength after cracking was approximately equal to 60% as opposed to 10–25% exhibited by the plain concrete beams. Varying the spacing between the stirrups from 200 mm to 150 mm did not significantly affect the maximum torque experienced by the specimens; that is, both the peak torque (Table 5) and the torque increment after cracking of the beams TB11, TB12, TB15, TB16 responded very similar to each other (Figure 6a). Furthermore, the results reported in Table 5 demonstrate that the beams containing fibers had a rotational capacity greater (>50%) than that of their plain concrete counterparts.

3.2 | Torsional rigidity

In order to highlight the variation of the rigidity after cracking, a polynomial interpolation was used to fit the responses previously presented in Figure 5. To perform the interpolation, either third or fourth order polynomials were selected, depending on which of the two provided the best fit of the experimental dataset. By way of

example, Figure 7 reports the Torque-twist curve of the specimen TB10-D50-L18 together with the interpolating functions used to approximate the response after cracking. It is seen that the third order polynomials were best suited to represent most of the actual curve except for the part included within the twist range $1.85–10.5 \times 10^{-3}$ rad/m, which required a fourth order function. The high value of the coefficients of determination (i.e., $R^2 > 0.98$) demonstrates that the adopted polynomials well fitted the experimental data.

The slope of the interpolating functions was calculated to estimate the torsional rigidity of the test specimens. The latter was normalized to the analytical value of the torsional rigidity (K_{DSV}) and is presented in Figure 8. To further clarify this comparison, the twist reported on the horizontal axis was normalized against the cracking twist Ψ'_{cr}. The obtained results are discussed in the following sections.

3.2.1 | Beams without stirrups

Figure 8a presents the torsional rigidity of all FRC specimens without stirrups aside for those (i.e., TB17 and TB18) which are characterized by low longitudinal reinforcement ratios. It is seen that after cracking the rigidity of the beams immediately dropped to values ranging from 3% to 30% of the rigidity K_{DSV} and then gradually decreased to zero as the specimens attained the maximum capacity.

As expected, the greatest loss of rigidity was exhibited by the two specimens TB7 and TB8 which contained

25 kg/m^3 of fiber Type "D." In fact, the sharp reduction of the residual flexural strength observed in the 3PBTs after first cracking (see Figure 3b) seems to correlate with the response of the large scale torsion specimens, which presented a quasi-horizontal torque-twist relationship (see Figure 5a) immediately after cracking. By increasing the fiber content to 50 kg/m^3, the torsional rigidity tripled in value as shown by the curves corresponding to specimens TB9 and TB10, whose normalized rigidity within the normalized twist range 1–3 varied from 11–14% to a minimum of 3–4%.

All the torsion specimens reinforced with Fiber Type "G" experienced a lower loss of rigidity, compared to Fiber Type "D," particularly in the normalized twist range 1–1.6. Within this range, the specimens TB7 and TB8 had normalized rigidities from 50% to 75% lower than those of the specimens TB3 and TB4. When the specimens TB5 and TB6 began to crack, their rigidities were about 120% higher than those of the specimens TB9 and TB10. Following initial cracking, the normalized rigidity of the four test specimens became very similar for normalized twists of about 1.6. Once the normalized twist achieved values greater than 3, all specimens presented normalized rigidities lower than 4%.

TB17 and TB18 are characterized by a low amount of longitudinal reinforcement and no transverse reinforcement. In spite of this, the addition of steel fibers to these specimens significantly mitigated the loss of rigidity after cracking. The ability of the two specimens to exhibit a stable and uniform response after cracking is clearly shown in Figure 8b.

3.2.2 | Beams with stirrups

Figure 8c presents the evolution of the post-cracking rigidity for the specimens containing transverse reinforcement. The rigidity of all specimens made with plain concrete were generally lower than that of the specimens which contained fibers. The latter were stiffer but, contrary to expectations, the rigidity of the four FRC specimens detected in the normalized twist range 1–3 was lower than that exhibited by the corresponding samples without stirrups (i.e., TB9 and TB10).

In specimens not containing fibers, the adoption of an increased stirrup spacing made the specimens TB13 and TB14 less stiff relative to TB2, especially within the normalized twist range 3–10. Contrarily, increasing the stirrup spacing from 150 mm to 200 mm did not significantly affect the response of the FRC specimens. In fact, the responses of the beams TB11 and TB12 are bounded by those of specimens TB15 and TB16 for the entire evolution of the curves.

3.3 | Analysis of crack patterns

3.3.1 | Crack distribution, orientation and slope

As discussed in Section 2.3, the evolution of the crack pattern was continuously monitored during the test through the potentiometers installed and mounted on the specimens. A DIC technique was also adopted for selected specimens. To further verify the results provided by the instrumentation, a handheld digital microscope was used to manually measure the width of all cracks periodically during testing.

Before the commencement of testing, a careful inspection of the specimens confirmed that the concrete was un-cracked.

The crack pattern of specimen TB1-PC consisted of a main localized diagonal/spiral crack that appeared after first cracking (at a load equal to $T_{cr} = 12.40$ kNm) and rapidly propagated through the monitored areas.

As noted in a previous study,[35] the FRC beams without stirrups presented a similar crack pattern evolution. At the onset of the post-peak descending branch of the torque-twist response (see Figure 5a), all critical torsional cracks were completely developed and stabilized. Very few new cracks appeared on the specimens as the torque decreased after peak load was attained. This explains why the specimens were not able to further resist an increase in the applied torsion. Failure of the specimens took place when the damage gradually localized in a single critical crack, leading to the progressive increase of its width, which corresponded in the progressive reduction of the torsional capacity. The increase of capacity after first cracking was due to the ability of the specimens to present enough ductility to develop multiple cracks and, therefore, to promote internal stress redistributions. By way of example, specimens TB3 and TB10, whose crack patterns consisted of many cracks dispersed through the entire surface of the specimens, reached a torque and twist capacity higher than those exhibited by the specimens TB7 and TB18, which developed notably fewer cracks (see Figure 9). The slope of each crack within each specimen was not constant as it was affected by the presence of conventional reinforcement located in the monitored region. Table 6 reports the mean angle of inclination of cracks (θ_v) measured at the mid-depth of the cross section. The inclination of the cracks ranged from a minimum of 40° to a maximum of 46°.

For the PC specimens, the inclusion of transverse reinforcement led to the development of multiple diagonal cracks that were not regularly spaced along the longitudinal axis of the beam (see TB2 and TB14 in Figure 9). The

FIGURE 9 Selected crack patterns detected at the maximum torque (crack pattern at failure only for TB2-PC-ST6/110 and TB3-D25-L18). (Dimensions in mm)
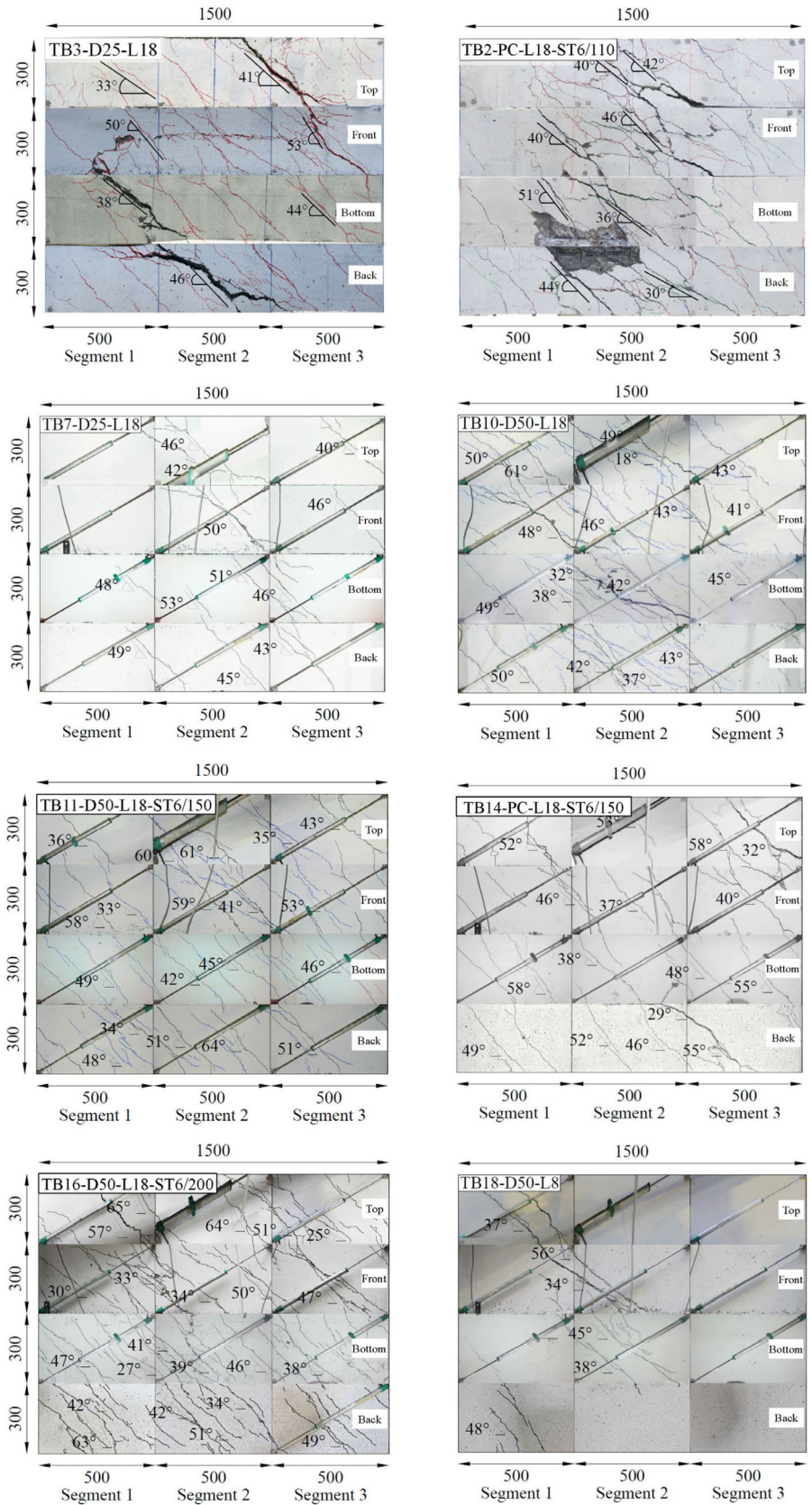
combination of fibers and stirrups generated an increase in the number of cracks, leading to a more diffused crack pattern (see beams TB11 and TB16 in Figure 9).

As observed for the specimens without stirrups, after first cracking, diagonal cracks continued to propagate and increase in number as the applied torque progressively

TABLE 6   Mean properties of cracks at peak torque

Specimen	θ_v (deg)	s_v (mm)	$w_{m,p}$ (mm)	$T_{0.3}$ (kNm)	$\Psi_{0.3}$ $\left(\frac{10^{-3}\,\text{rad}}{\text{m}}\right)$
TB1-PC-L18	43[a]	—	0.04	—	—
TB2-PC-L18-ST6/110	42[a]	140[a]	0.14[a]	18.8	20
TB3-G25-L18	43[a]	185[a]	0.29[a]	27.3	19
TB4-G25-L18	41[a]	310[a]	0.25[a]	22.5	13
TB5-G50-L18	46[a]	160[a]	0.18[a]	26.6	16
TB6-G50-L18	45[a]	175[a]	0.20[a]	24.3	20
TB7-D25-L18	45	265	0.21	19.9	8
TB8-D25-L18	42	360	0.14	19.9	6
TB9-D50-L18	42	115	0.15	27.3	21
TB10-D50-L18	41	140	0.25	24.7	25
TB11-D50-L18-ST6/150	44	130	0.44	33.5	22
TB12-D50-L18-ST6/150	46	140	0.48	30.6	19
TB13-PC-L18-ST6/150	45	210	0.24	20.9	15
TB14-PC-L18-ST6/150	47	230	0.35	20.8	13
TB15-D50-L18-ST6/200	45	120	0.54	30.9	18
TB16-D50-L18-ST6/200	43	90	0.37	32.5	26
TB17-D50-L8	45	330	0.64	21.6	7
TB18-D50-L8	40	180	0.30	21.9	8

[a]Mean slope (θ_v), spacing (s_v) and width ($w_{m,p}$) of the cracks forming the ultimate damage pattern.

approached peak load. In the post-peak stage, many secondary cracks developed that led to spalling of concrete surrounding the longitudinal reinforcement. We note, however, that the presence of the fibers significantly mitigated this phenomenon and prevented the total detachment of concrete cover. The mean crack inclination detected for both the FRC and the PC beams with stirrups was in general very close to 45° (see Table 6).

3.3.2 | Crack width and spacing

To determine the average crack spacing (s_v) at peak load, the mean distance between the cracks at the mid-depth of the section was measured. These results are summarized for each specimen in Table 6. Note that the crack spacing of the specimens included in Test Series 1 (i.e., specimens TB1 to TB6) were determined by considering the number of cracks detected at failure rather than at peak load. However, the crack spacing of the two Test Series are comparable as the number of main cracks observed at peak load and at the end of the test were approximately the same. For the FRC beams without stirrups and reinforced with Ø18 longitudinal bars, the crack spacing appears proportional to the FRC toughness, which is related to the fiber content. As observed in other studies,[42–44] an increase in the supplied fiber dosage in

lightly reinforced FRC elements leads to a reduction of the average spacing of cracks. Averaging the two values of s_v obtained for the beams containing 50 kg/m^3 of fibers "D" and "G" gives the average crack spacing equal to 128 mm and 168 mm, respectively. For specimens containing 25 kg/m^3 of fibers, the average crack spacing increases to 313 mm and 250 mm, respectively.

The values of s_v observed for the two specimens with Ø8 longitudinal reinforcement differ considerably from each other. It is worth noting that the average crack spacing (i.e., s_v = 255 mm) of these beams was between that of the beams made with 25 kg/m^3 (i.e., TB7 and TB8) and 50 kg/m^3 (i.e., TB9 and TB10) of Type "D" fibers.

The influence of stirrup spacing on crack spacing was evident. The specimens TB11 and TB12, which were provided with the same stirrup arrangement as that in specimensTB13 and TB14, had an average crack spacing of 135 mm. In this case, the addition of 50 kg/m^3 fibers led to a 40% reduction of crack spacing. Contrary to expectations, an increase of stirrup spacing to s_{st} = 200 mm in the FRC beams TB15 and TB16 led to a 20% reduction of the crack spacing as compared to the specimens TB13 and TB14.

The use of DIC in the present testing allows for a point-by-point critical assessment on the distribution of crack widths along the length of the crack. Figure 10 presents a contour of crack widths detected at peak torque on the front side of selected specimens. In this crack

FIGURE 10 Distribution of crack width according to DIC analysis performed at peak torque (crack width in mm)
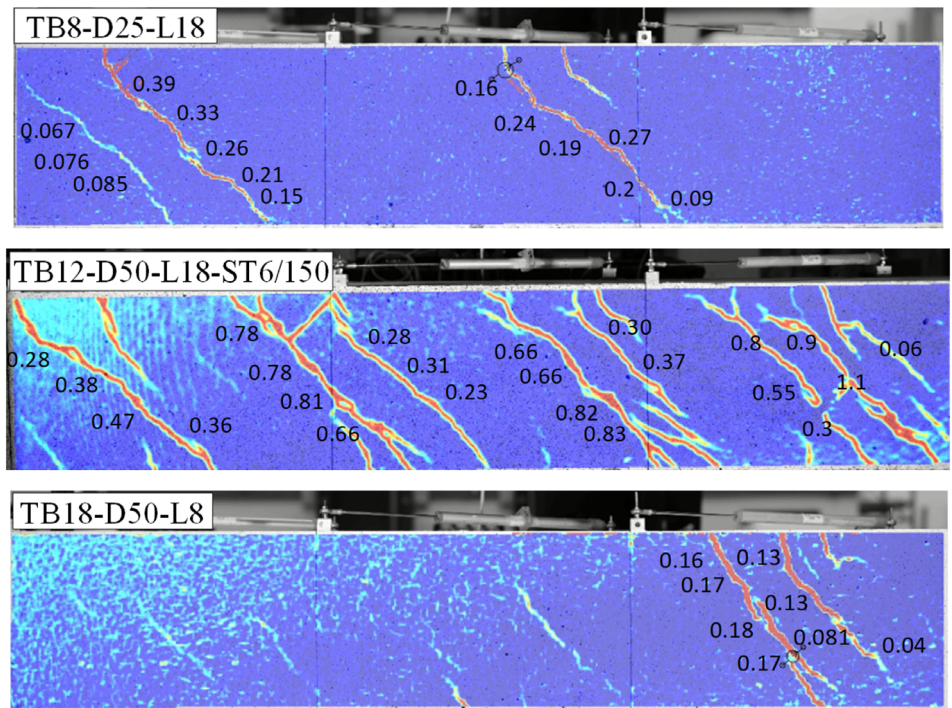
contour, the color red represents the widest cracks whereas the color white represents the narrowest cracks. The dark blue background represents the undamaged areas. The results confirm that the FRC beams containing stirrups exhibited cracks wider than those observed on the specimens without stirrups at peak load, as generally the specimens containing stirrups reached loads greater than specimens without stirrups. However, we note that at peak load, the maximum crack width was rarely greater than 0.8 mm. Moreover, it is interesting to note that the width of cracks varied only slightly along the length of the crack, irrespective of the type of specimen considered in the contour.

The estimation of the mean crack width ($w_{m,p}$) at peak torque, including cracks detected on all the sides of the specimens, is reported in Table 6. At peak torque, the mean crack widths for the FRC beams without stirrups ranged from 0.15 mm to 0.25 mm. In the FRC beams with stirrups, the minimum and the maximum cracks widths increased to 0.40 mm and 0.50 mm, respectively.

Finally, to compare the actual relative performance of the specimens, Table 6 also reports the torque ($T_{0.3}$) and the corresponding twist ($\Psi_{0.3}$) detected when the overall mean crack width was equal to 0.3 mm. This value was chosen as it is generally assumed as a permissible (or maximum design) crack width limit for concrete structures under service conditions. The results show that the FRC specimens without stirrups already attained their maximum capacity when the mean crack width was about 0.3 mm. In fact, the torque $T_{0.3}$ is very close to the peak value (T_p) reported in Table 5. As the tensile

performance of FRC and the number of cracks increased, the value of $\Psi_{0.3}$ also increased. By way of example, the twist $\Psi_{0.3}$ of the specimens with the largest number of cracks (i.e., TB3 and TB6) was more than double than that of the specimens TB7, TB8, TB17 and TB18.

Cracks with a width of 0.3 mm appeared on the specimens with stirrups well before attaining peak torque. Depending on the stirrup spacing, the torque $T_{0.3}$ of the four FRC beams was at least 47% higher than that of their PC counterparts. When combining fibers with stirrups, the increment of $\Psi_{0.3}$ with respect to the PC beams seems less pronounced (i.e., ≈50%) than that experienced by the FRC beams without stirrups.

4 | CONCLUDING REMARKS

This paper presents the results of an experimental campaign intending to investigate the response of large-scale SFRC beams subjected to pure torsion. Eighteen specimens containing varying amounts of transverse and longitudinal reinforcement along with varying steel fiber types and dosages were manufactured and tested to failure. Based on the experiments and discussion reported herein, the following key conclusions are drawn:

- The addition of fibers is an effective means of replacing conventional transverse reinforcement. Specimens containing fibers provided a stable response after peak load was achieved, even for specimens containing low amounts of longitudinal reinforcement.

- When fibers are included in specimens containing transverse reinforcement, cracks become more dispersed and finer. This leads to greater ductility in the specimens which is characterized by greater rotations and strengths at peak load. At peak torque, the mean crack widths for the FRC beams without stirrups ranged from 0.15 mm to 0.25 mm. For the SFRC beams with stirrups, the minimum and the maximum cracks widths increased to 0.40 mm and 0.50 mm, respectively.

- The FRC specimens without stirrups presented a considerable torsional rigidity after cracking. For twist values varying from 1 to 2 times the cracking twist, the torsional rigidity ranged from a minimum of 0.04 to a maximum of 0.3 times the initial elastic rigidity. Within the same twist range, the specimens containing both stirrups and fibers presented similar normalized rigidities.

- After initial cracking, specimens containing both fibers and stirrups were stiffer than the corresponding beams containing only stirrups. In fact, the normalized rigidity of the former was about two times higher than the latter one.

- The inclination of the cracks ranged between 40° and 46° and did not appear to be significantly influenced by the FRC toughness, or with the quantity of transverse reinforcement.

- The presence of fibers significantly mitigated the detrimental effects that can be induced through the spalling of concrete and prevented the total detachment of the concrete cover from the core of the beam, even at very large rotations.

These conclusions will be used to inform the model presented in the accompanying paper.[36]

CONFLICT OF INTEREST

The authors declare that they have no conflict of interest.

DATA AVAILABILITY STATEMENT

The data that support the findings of this study are available from the corresponding author upon reasonable request.

ORCID

Luca Facconi https://orcid.org/0000-0003-2202-5439
Ali Amin https://orcid.org/0000-0002-9088-8634
Fausto Minelli https://orcid.org/0000-0002-4554-4285
Giovanni Plizzari https://orcid.org/0000-0003-2897-4969

REFERENCES

1. fib Model Code for Concrete Structures 2010. October 2013. 434 pp. ISBN: 978-3-433-03061-5.
2. di Prisco M, Plizzari G, Vandewalle L. Fibre reinforced concrete: new design perspectives. Mater Struct. 2009;42:1261–81.
3. Minelli F. Plain and fibre reinforced concrete beams under shear loading: structural behavior and design aspects. PhD dissertation. Italy: Department of Civil Engineering, University of Brescia; 2005.
4. Löfgren I. Fibre-reinforced concrete for industrial construction—a fracture mechanics approach to material testing and structural analysis. PhD dissertation. Sweden: Department of Civil and Environmental Engineering, Chalmers University of Technology; 2005.
5. Amin A, Gilbert RI. Steel fibre-reinforced concrete beams—part I: material characterization and in-service behavior. ACI Struct J. 2019;116(2):101–12.
6. Minelli F, Vecchio FJ. Compression field modelling of fibre reinforced concrete members under shear loading. ACI Struct J. 2006;103(2):244–52.
7. Maya LF, Ruiz MF, Muttoni A, Foster SJ. Punching shear strength of steel fibre reinforced concrete slabs. Eng Struct. 2012;40:83–94.
8. Soltanzadeh F, Edalat-Behbahani A, Barros JA, Mazaheripour H. Effect of fibre dosage and prestress level on shear behavior of hybrid GFRP-steel reinforced concrete I-shape beams without stirrups. Compos Part B: Eng. 2016;102:57–77.
9. Amin A, Foster SJ. Shear strength of steel fibre reinforced concrete beams with stirrups. Eng Struct. 2016;111:323–32. https://doi.org/10.1016/j.engstruct.2015.12.026
10. Facconi L, Minelli F. Behavior of lightly reinforced fibre reinforced concrete panels under pure shear loading. Eng Struct. 2020;202:109879.
11. de Montaignac R, Massicotte B, Charron JP. Design of SFRC structural elements: flexural behaviour prediction. Mater Struct. 2012;45(4):623–36. https://doi.org/10.1617/s11527-011-9785-y
12. Mobasher B, Yao Y, Soranakom C. Analytical solutions for flexural design of hybrid steel fibre reinforced concrete beams. Eng Struct. 2015;100:164–77.
13. di Prisco M, Colombo M, Pourzarabi A. Biaxial bending of SFRC slabs: is conventional reinforcement necessary? Mater Struct. 2019;52(1):1.
14. Facconi L, Plizzari G, Minelli F. Elevated slabs made of hybrid reinforced concrete: proposal of a new design approach in flexure. Struct Concr. 2019;20(1):52–67.
15. Amin A, Gilbert RI. Steel fibre reinforced concrete beams—part II: strength, ductility, and design. ACI Struct J. 2019;116(2):113–24.
16. Cugat V, Cavalaro SHP, Bairán JM, de la Fuente A. Safety format for the flexural design of tunnel fibre reinforced concrete precast segmental linings. Tunnel Underground Space Technol. 2020;103:103500.
17. Markic T, Amin A, Kaufmann W, Pfyl T. Strength and deformation capacity of tension and flexural RC members containing steel fibres. J Struct Eng. 2020;146(5):04020069-1–04020069-17.
18. Deluce JR, Vecchio FJ. Cracking behavior of steel fibre-reinforced concrete members containing conventional reinforcement. ACI Struct J. 2013;110(3):481–490.
19. Vasanelli E, Micelli F, Aiello MA, Plizzari G. Crack width prediction of FRC beams in short and long term bending condition. Mater Struct. 2014;47(1–2):39–54.
20. Fantilli AP, Cavallo AD, Pistone G. Fibre-reinforced lightweight concrete slabs for the maintenance of the Soleri viaduct. Eng Struct. 2015;99:184–91.
21. Chilwesa M, Facconi L, Minelli F, Reggia A, Plizzari G. Shrinkage induced edge curling and debonding in slab elements

reinforced with bonded overlays: influence of fibres and SRA. Cem Concr Compos. 2019;102:105–15.

22. Tiberti G, Trabucchi I, AlHamaydeh M, Minelli F, Plizzari GA. Crack development in steel-fibre-reinforced concrete members with conventional rebars. Mag Concr Res. 2019;71(11):599–610.

23. Watts MJ, Amin A, Gilbert RI, Kaufmann W, Minelli F. Simplified prediction of the time dependent deflection of SFRC flexural members. Mater Struct. 2020;53:1–11.

24. AS3600, Concrete structures. Australian standard, standards association of Australia, 2018.

25. AS 5100.5, Australian standard, bridge design part 5: concrete, standards Australia, Sydney, Australia, 2017.

26. NZS 3101: Part 2, Concrete structures standard part 2 – commentary on the design of concrete structures. Wellington, New Zealand: Standards New Zealand; 2006.p. 391.

27. ACI Committee 318. Building code requirements for structural concrete (ACI 318-08) and commentary (ACI 318-08). Farmington Hills, MI: American Concrete Institute; 2008.p. 473.

28. ACI Committee 544. Report on fibre reinforced concrete (ACI 544.1R-96). Farmington Hills, MI: American Concrete Institute; 2009.p. 63.

29. Mansur MA, Paramasivam P. Steel fibre reinforced concrete beams in pure torsion. Int J Cem Compos Lighw Concr. 1982;4(1):39–45.

30. Narayanan R, Kareem-Palanjian AS. Torsion in beams reinforced with bars and fibres. J Struct Eng. 1986;112(1):53–66.

31. Rao TDG, Seshu DR. Torsion of steel fibre reinforced concrete members. Cem Concr Res. 2003;33(11):1783–8.

32. Chalioris CE, Karayannis CG. Effectiveness of the use of steel fibres on the torsional behaviour of flanged concrete beams. Cem Concr Compos. 2009;31(5):331–41.

33. Yang IH, Joh C, Lee JW, Kim BS. Torsional behavior of ultra-high performance concrete squared beams. Eng Struct. 2013;56:372–83.

34. Amin A, Bentz EC. Strength of steel fibre reinforced concrete beams in pure torsion. Struct Concr. 2018;19(3):684–94.

35. Facconi L, Minelli F, Ceresa P, Plizzari G. Steel fibres for replacing minimum reinforcement in beams under torsion. Mater Struct. 2021;54:34. https://doi.org/10.1617/s11527-021-01615-y

36. Facconi L, Amin A, Minelli F, Plizzari G. A unified approach for determining the strength of FRC members subjected to torsion – part II: analytical modelling. Submitted. Struct Concr. 2021. https://doi.org/10.1002/suco.202100162

37. EN 1992-1-1 Eurocode 2: Design of concrete structures – Part 1-1: General rules and rules for buildings. E. for Standardization. Brussels, EN, CEN, (2005) EC2.

38. UNI EN 14651:2007, Test method for metallic fibre concrete – Measuring the flexural tensile strength (limit of proportionality (LOP), residual), 2007.

39. ISO 15630-1. Steel for the reinforcement and prestressing of concrete – Test methods – Part 1: Reinforcing bars, wire rod and wire, 2010

40. Desai N. Small-strain measurement in bridges using the digital image correlation (DIC) technique. In: Proc. SPIE 9805, Health Monitoring of Structural and Biological Systems, Las Vegas, NV, 2016.

41. Collins MP, Mitchell D. Prestressed concrete basics. Ottawa, Ontario: Canadian Prestressed Concrete Institute; 1987.

42. Chiaia B, Fantilli AP, Vallini P. Crack patterns in reinforced and fibre reinforced concrete structures. Open Construct Build Technol J. 2008;2(1):146–155.

43. Lee SC, Cho JY, Vecchio FJ. Tension-stiffening model for steel fibre-reinforced concrete containing conventional reinforcement. ACI Struct J. 2013;110(4):639–648.

44. Bernardi P, Michelini E, Minelli F, Tiberti G. Experimental and numerical study on cracking process in RC and R/FRC ties. Mater Struct. 2016;49(1–2):261–77.

AUTHOR BIOGRAPHIES

Luca Facconi,
Department of Civil, Environmental, Architectural Engineering and Mathematics (DICATAM), University of Brescia, Brescia, Italy.
Email: luca.facconi@unibs.it

Ali Amin,
School of Civil Engineering, The University of Sydney, Sydney, Australia.
Email: ali.amin@sydney.edu.au

Fausto Minelli,
Department of Civil, Environmental, Architectural Engineering and Mathematics (DICATAM), University of Brescia, Brescia, Italy.
Email: fausto.minelli@unibs.it

Giovanni Plizzari,
Department of Civil, Environmental, Architectural Engineering and Mathematics (DICATAM), University of Brescia, Brescia, Italy.
Email: giovanni.plizzari@unibs.it